TECHNICAL NOTE
D-47

DYNAMIC ANALYSIS OF A SIMPLE REENTRY MANEUVER FOR A LIFTING SATELLITE

By Frederick C. Grant

Langley Research Center
Langley Field, Va.

NATIONAL AERONAUTICS AND SPACE ADMINISTRATION

WASHINGTON September 1959

NATIONAL AERONAUTICS AND SPACE ADMINISTRATION

TECHNICAL NOTE D-47

DYNAMIC ANALYSIS OF A SIMPLE REENTRY MANEUVER FOR A LIFTING SATELLITE

By Frederick C. Grant

SUMMARY

The dynamic properties of a simple reentry maneuver are presented. The maneuver is designed to put the reentry vehicle on a smooth glide trajectory after a single skip. This maneuver is accomplished by a properly chosen zero-lift coasting period. The chosen coasting period satisfies general boundary conditions at the start of the glide. Wing loadings of 20 and 100 pounds per square foot are considered for reentry angles up to 6° with a lift-drag-ratio range of 1/2 to 5. Reentry speeds corresponded to the energy levels of circular orbits at 655,000 and 490,000 feet.

The simple single-skip maneuver was possible over a wide range of the parameters considered but, naturally enough, was easiest at low lift-drag ratios. The effects of wing loading were generally small. The higher lift-drag-ratio maneuvers were possible only at the higher reentry angles. The minimum reentry angle for a successful maneuver at a high lift-drag ratio was sharply reduced by the lower energy level. The precision of the maneuver was found to be highly sensitive to the time of the start of the coast and less so to the time of lift restoration. Coasting distances of less than 1,000 nautical miles were only possible for lift-drag-ratio values under about 2.

Maximum normal accelerations had a roughly parabolic variation with reentry angle. The highest value calculated was 4.7g at a lift-drag ratio of 5 for a wing loading of 100 pounds per square foot and a reentry angle of 6°.

INTRODUCTION

General problems of heating and reentry have received extensive treatment as, for example, in references 1 to 3. For a lifting satellite, there is the special question of the manner in which the available aerodynamic forces should be used to achieve transition from flight under

gravitational forces to flight under gravitational and aerodynamic forces. Some consideration of this problem is given in references 4 and 5 for continuously variable lift.

This paper will consider a special case of transition to what is usually called a glide trajectory. Transition will be made in a simple maneuver which may be called a lift-coast-lift maneuver. The vehicle pulls up at constant lift coefficient as it reenters the atmosphere. At a properly chosen moment past the bottom of the pullup, the lift is suddenly cut to zero and the vehicle coasts essentially under gravity. After another properly chosen interval the lift is restored and the vehicle is then in a smooth glide. The dynamic properties of this maneuver will be investigated for a range of initial conditions and vehicle properties. Most consideration will be given to lift-drag ratio, reentry angle, and wing loading.

L
2
5
9

SYMBOLS

Physical variables:

t	time
T	kinetic energy
W	sea-level weight $(m\underline{g})$; gravitational potential of satellite $(W = 0 \text{ for } \bar{H} = \infty)$
H	altitude
h_o	arbitrary reference altitude
S	arbitrary reference area of vehicle
ρ	air density
m	mass of vehicle
V	velocity of vehicle
V_s	velocity of gravitational satellite at altitude h_o

Physical constants:

$\underline{g}$	acceleration of gravity at surface of earth, 32.18 ft/sec^2
R	radius of the earth, 3,957 miles

Dimensionless variables:

τ	time parameter, $\frac{V_s t}{h_o}$
ν	velocity parameter, $\frac{V}{V_s}$
θ	angle of velocity above local horizontal, radians
χ	acceleration of gravity, $\frac{h_o}{V_s^2} \frac{g}{\left(1 + \frac{H}{R}\right)^2}$
ω^{-1}	distance from center of earth, $\frac{R + H}{h_o}$
λ	lift parameter, $\frac{Sh_o}{2m} \rho C_L$
δ	drag parameter, $\frac{Sh_o}{2m} \rho C_D$
Ψ	angular position along surface of the earth, radians
η	altitude above surface of the earth, $\frac{H}{h_o}$
$\bar{\eta}$	orbital altitude above surface of the earth, $\frac{\overline{H}}{h_o}$
D	arbitrary reference height, $\frac{h_o}{R}$
L/D	lift-drag ratio
C_L	lift coefficient
C_D	drag coefficient
Γ	energy constant, $\frac{T + W}{\frac{1}{2} mV_s^2}$
K	Kepler's constant of area, $\left(1 + \frac{H}{R}\right)\frac{V}{V_s} \cos \theta$

F discriminant function

β logarithmic decrement of density with η, $\frac{d}{d\eta}(-\log_e \rho)$

Subscripts:

C lift cutoff

R lift restoration

1 initial value

A bar over a symbol denotes that the variable is evaluated at orbital altitude. A primed symbol denotes a derivative with respect to τ.

Dots over symbols denote derivative with respect to t.

ANALYSIS

Idealized Motion

Consider the motion illustrated schematically in figure 1. The wave-like curve marked H represents a vehicle with a constant lift coefficient and no drag or thrust moving in the atmosphere. This motion is the classical phugoid motion. The sum of the kinetic energy T and gravitational potential energy W is constant just as in a free falling motion. The curve $\bar{H}$ defines the orbital altitude, which is the height for which a sudden change of velocity to the horizontal direction results in a constant-altitude path. The value of $\bar{H}$ depends only on the energy constant of the motion for a given ratio of lift coefficient to wing loading.

If the lift coefficient is allowed to vary, a simple maneuver will produce the same constant-altitude flight as a sudden change in velocity direction at $\bar{H}$. At the point marked C in figure 1 the lift is suddenly reduced to zero and the vehicle coasts on an arc of an ellipse. If C is properly chosen, apogee will occur at $\bar{H}$ and restoration of the lift results in constant-altitude flight from R.

Real Motion

If finite drag is introduced, the periodic motion of figure 1 becomes the familiar damped skipping oscillation. The altitude $\bar{H}$ continually

diminishes and the amplitude of the H oscillation diminishes. Eventually a steady glide results. The tendency of H to oscillate about $\bar{H}$ persists through the entire motion.

If zero drag is now assumed only in the coast and the maneuver of figure 1 is repeated, the new conditions at R are shown in figure 2. The variation of $\bar{H}$ with time now has a finite negative slope beyond R and the separation of H and $\bar{H}$ will initially increase. This condition is unsatisfactory if a smooth glide is desired beyond R, since conditions favorable to oscillation are obtained at R.

In order to define precisely the conditions favorable to gliding motion beyond R, it is only necessary to look at the last part of the damped skipping oscillation where a smooth glide is known to occur. This part of the motion, near the earth at low speed in air of constant density, is indicated in figure 3. The interval $H - \bar{H}$ may be readily shown to be

$$H - \bar{H} = \frac{1}{2}\frac{V^2}{g}\left(\frac{1}{\cos\theta} - 1\right) \tag{1}$$

The tendency of H to move toward $\bar{H}$ persists, as can be seen in figure 3. Now, however, $\bar{H}$ is dropping as fast as H and there is no oscillation. This property of the gliding motion may be written as

$$\dot{H} = \dot{\bar{H}} \tag{2}$$

The straightness of the glide path can be stated by the condition

$$\dot{\theta} = 0 \tag{3}$$

If conditions (2) and (3) are now transferred to R and satisfied there, the motion beyond R will be, to the first order in the time, a smooth glide.

Consider now the maneuver outlined in figure 4 which satisfies the condition $\dot{H} = \dot{\bar{H}}$ but not the condition $\dot{\theta} = 0$. Zero coast drag is still assumed. After lift cutoff at C the vehicle coasts upward past $\bar{H}$ and the lift is restored when $H = \bar{H}$ the second time. The condition $H = \bar{H}$ occurs at a slightly lower altitude than the condition $\dot{\theta} = 0$. For a neighborhood of R in which θ and ν can be assumed constant, the increment in altitude between $\bar{H}$ and H for $\dot{\theta} = 0$ can be approximated as

$$\frac{\Delta H}{h_o} = \Delta\eta = \frac{\bar{\theta}^2}{2\beta} \tag{4}$$

where

$$\beta = - \frac{d(\log_e \rho)}{d\eta}$$

In equation (4), $\bar{\theta}$ is assumed to be so small that $\bar{\theta} = \sin \bar{\theta} = \tan \bar{\theta}$ and $\cos \bar{\theta} = 1$. For $\bar{\theta} = 1^\circ$, $\Delta H \approx 3$ feet. The values of $\bar{\theta}$ are usually much less than 1°. To a high approximation, then, the condition $\dot{\theta} = 0$ occurs at $H = \bar{H}$ for the usual reentry conditions. The modified boundary conditions at R are thus

$$\left.\begin{aligned} H &= \bar{H} \\ \dot{H} &= \dot{\bar{H}} \end{aligned}\right\} \qquad (5)$$

L 2 5 9

For high L/D ratios the coasting drag coefficient will be about one-half the gliding drag coefficient. For an L/D near unity, corresponding to an angle of attack of about 45°, the coast drag coefficient may be more like 1/20 of the gliding drag coefficient. If C is chosen at the same time as for zero coast drag and R is chosen again at $H = \bar{H}$, the condition $\dot{\theta} = 0$ will again be nearly satisfied, but the condition $\dot{H} = \dot{\bar{H}}$ is disturbed and $\dot{H} \neq \dot{\bar{H}}$ at R.

By using the zero drag trajectories as a basis, it is possible to compute the shift in C required to satisfy conditions of equations (5). Calculations have shown that the effect of ignoring the finite coast drag is similar to the effect of a piloting error in the position of C. The effect of inexact maneuvering is shown subsequently.

RESULTS

Calculations

Results of digital-computer calculations of the lift-coast-lift maneuver, idealized by the assumption of zero coast drag, are given in figures 5 to 8. Details of the calculations are given in the appendix.

The vehicle considered is one with a maximum lift-drag ratio of 5 and a minimum drag coefficient of 0.004. This assumed vehicle thus has a high L/D capability. The lift-drag relation is assumed to be parabolic with the form

$$C_D = 0.004 + 2.5C_L^2 \qquad (6)$$

For L/D values less than 5, the vehicle is presumed to operate on the high-lift—high-drag side of maximum L/D. In order to span a range of practical interest, calculations were made for wing loadings of 20 and 100 pounds per square foot. The C_L, C_D, and W/C_DS values used are listed in table I. All calculations were for two initial velocities and one initial altitude, namely,

$$V_1 = 25{,}900 \text{ and } 25{,}800 \text{ fps}$$

$$H_1 = 350{,}000 \text{ ft}$$

The lower V_1 value is about 85 feet per second higher than satellite speed at 350,000 feet. Expressed another way, the circular orbit heights for these energy levels are about 655,000 and 490,000 feet. All calculations are for the ARDC atmosphere. (See ref. 6.) Reentry angles were varied to a maximum of 6°.

In figure 5, the variations of θ_C and θ_R with reentry angle $-\theta_1$ are shown for both initial velocities. A single curve is drawn to represent the entire range of wing loadings of 20 pounds per square foot to 100 pounds per square foot for every case except L/D = 1/2. The deviation from the single curves shown is always less than about 0.05° in the case of θ_C and 0.01° in the case of θ_R. The curves for the L/D values other than 1/2 are all terminated at the lower reentry angles by vertical lines. These lines mark the reentry angles for which local satellite speed is attained at the bottom of the pullup. This apparently arbitrary termination of the curves actually occurs very near the end of the range of practicality of the maneuver. For slightly lower reentry angles than those marked by the vertical lines, the velocity is higher than local satellite speed in the bottom of the pullup and very small θ_C values are required. This condition occurs because a certain altitude rise is assured even if the coast is started when $\theta = 0^\circ$. For still lower reentry angles and higher speeds at the minimum altitude, the single-skip maneuver becomes impossible for the kind of maneuver under consideration. In these cases, even for $\theta_C = 0^\circ$, the apogee height is so great that the condition $\dot{H} = \bar{\dot{H}}$ is not satisfied at $H = \bar{H}$, but at a much higher altitude.

These considerations must be modified for the lower values of L/D. Figure 5 suggests that the case of L/D = 1/2 is distinct from the others. For such a low lift-drag ratio the vehicle motion is more nearly that of a drag vehicle perturbed by lift forces rather than that of a lifting vehicle damped by drag forces. The anomalous character of the L/D = 1/2 curves as compared with the higher L/D curves thus seems reasonable.

The chief effect of the lower reentry velocity is to reduce substantially the minimum reentry angles at which the maneuver is possible at the higher L/D values.

The maximum normal air loads experienced in the maneuver are summarized in figure 6. These loads occur just before the bottom of the pullup. All the data for both initial velocities fall within the indicated bands. Only at the higher angles is there an appreciable difference in the effects of L/D for the extremes of wing loading. The mean values of normal air loading are not too different, but the effect of L/D is rather less for the lightest wing loading than for the heaviest wing loading at the highest reentry angles. A mean line through the indicated bands has a roughly parabolic variation with reentry angle. The detailed results are somewhat dependent on the simple aerodynamic model chosen. However, the range of the parameter W/C_LS has a 5:1 ratio of high value to low which insures that the bands of figure 6 represent a wide range of actual aerodynamic characteristics.

In figure 7 the coasting times and corresponding coasting distances are indicated. The quarter-satellite-period coasting times are indicated for the angles at which satellite speed occurs at the minimum altitude. The basis for this choice is that, when local satellite speed occurs precisely at lift cutoff, the apogee point is 90° ahead of the position at cutoff. The changes in apogee position with velocity are so rapid in the neighborhood of satellite speed that these quarter-period values should be regarded as marking the onset of very long coast periods approaching full satellite periods for the fast, shallow, high L/D reentries which necessarily require more than a single skip for reentry. The distance scale shown on the right matches the quarter-period time to the quarter-circumference distance. This value is not quite correct for the lowest L/D values but on the scale of the plot is a negligible defect. The important feature is that only at L/D values less than about 2 are coasting distances under 1,000 nautical miles possible. The small effect of wing loading is also apparent. The effect of the lower reentry speed is a significant decrease in coasting time and distance, particularly at the lower reentry angles.

In figure 8 the data defining the altitudes at which the glide starts are summarized. Two bands are indicated, each for an extreme of wing loading. Starting at the highest reentry angles, the altitude bounds are indicated for all the data. At the lower angles the points corresponding to satellite speed at minimum altitude are indicated. These points were taken as the upper boundary of the altitude bands in the lower reentry angle range. The bottom line of each band defines the data for $L/D = 1/2$. The altitude bands have been arbitrarily cut off at a reentry angle of 1° and at $\bar{H}$ equal to 305,000 and 280,000 feet.

The bands thus cover almost the entire range of single-skip reentries. In figure 8 only a gradual change of $\bar{H}$ with reentry angle for a given L/D and a small effect of initial velocity are shown. It is plain that the main effect of lower initial velocity is to increase the range of reentry angle which allows a successful maneuver.

Figure 9 shows the velocities and altitudes calculated at the bottom of the pullups. Comparison of results for the same wing loading shows little effect of initial velocity. The changes due to wing loading are more pronounced, the heavier vehicle having the deeper penetration. On the basis of the analysis of reference 1, the velocity in the bottom of the pullup is given by

$$V = V_1 e^{\frac{D}{L}\theta_1} \tag{7}$$

Figure 9 indicates that formula (7) is a good approximation if L/D = 1/2 is excluded. Cases for which the speed increases in the pullup are not indicated by formula (7). However, these cases fall within the limits of accuracy (better than 2 percent) observed in figure 9 for formula (7).

Precision of Maneuver

The effect of incorrect lift cutoff is shown in figure 10 which is a plot of the variation of flight-path angle θ with time. The solid curve marked B is a perfect maneuver. The curves marked A and C indicate the start of the motion after lift restoration when the coast was started 3.9 seconds early for A and 3.9 seconds late for C. The coast periods for cases A and C are not indicated since they lie so close to the precise coasting maneuver B. The continuations of A and C have been omitted for clarity, but the calculations show that the A and C phugoid oscillations damp slowly into curve B and are very close to B beyond 30 minutes. For all three cases the condition $H = \bar{H}$ was satisfied at lift restoration, but $\dot{\bar{H}} \neq \dot{H}$ in cases A and C. Case A is a perfect maneuver for the case of zero gliding drag (fig. 1), since the flight path is horizontal at lift restoration. The resultant wobble in θ for case A can be regarded as the result of ignoring the nonzero gliding drag. Calculations have shown that, in case C, the amplitude of θ wobble can be reduced by restoring the lift somewhat sooner in order to improve satisfaction of $\dot{H} = \dot{\bar{H}}$ while relaxing the condition $H = \bar{H}$. The precision of the maneuver is evidently very sensitive to the time of lift cutoff. In any practical case, therefore, some θ wobble will undoubtedly remain to be eliminated after lift restoration by a pilot or automatic means. Even the 0.4-second integration interval was too large to prevent wobble in some of the calculations.

For a finite coast drag, lift cutoff at the correct time for zero coast drag and restoration at $H = \overline{H}$ will introduce an error into the satisfaction of $\dot{\overline{H}} = \dot{H}$. A wobble in θ will thus result. This wobble may be eliminated by a small shift in cutoff time depending on the amount of the coasting drag. Similarly, the effect of using an incorrect variation of density with altitude will disturb the satisfaction of the boundary conditions and a phugoid wobble in θ will result. The accelerations associated with the θ variations exhibited in figure 9 are very small. In a dynamical sense then the maneuvers of figure 9 may all be considered to be equivalent and the effect of the imprecise maneuvering may be considered to be negligible.

Since the flight-path angles are small, a constant-attitude reentry is nearly a constant angle-of-attack maneuver. If the vehicle is required to hold a constant attitude in the pullup and another constant attitude in the coast, a close resemblance to the idealized maneuver of figure 4 is achieved. The finite times required for attitude change, the nonzero lift and drag in the coast, and the small variations in lift and drag coefficient during the pullup may all be regarded as perturbations on the idealized zero-coast-drag maneuver with instantaneous lift cutoff and restoration. Thus, a realistic coasting maneuver can be tailored to a specific vehicle by starting with the idealized motion and correcting the lift cutoff C and lift restoration R by iteration.

L 2 5 9

CONCLUDING REMARKS

Analysis of one of the simplest reentry maneuvers, the lift-coast-lift maneuver, illustrates the boundary conditions which must be satisfied at the end of any transition to glide maneuver. For the simple maneuver, numerical calculations applying the proper boundary conditions to a simple analytical representation of a reentry vehicle have indicated the values of the angles for lift cutoff and restoration, coasting times, coasting distances, and accelerations associated with a range of wing loadings and reentry angles for the simple maneuver.

The simple single-skip maneuver was possible over a wide range of the parameters considered but, naturally enough, was easiest at low lift-drag ratios. The effects of wing loading were generally small. The higher lift-drag-ratio maneuvers were possible only at the higher reentry angles. The minimum reentry angle for a successful maneuver at a high lift-drag ratio was sharply reduced by the lower energy level. The precision of the maneuver was found to be highly sensitive to the time of the start of the coast and less so to the time of lift restoration. Coasting distances of less than 1,000 nautical miles were only possible for lift-drag-ratio values under about 2.

Removal of the idealizations assumed in the analysis slightly shifts the required lift-cutoff and lift-restoration times. The effect of small errors in performance of a desired lift program is to introduce a phugoid wobble into the final glide-angle variation with time. Although consideration has been given only to constant lift-drag ratio pullups and glides, it is obvious that a low lift-drag pullup can be matched to a high lift-drag glide, and vice versa. Such combinations introduce glide stretching and cutting possibilities.

Langley Research Center,
National Aeronautics and Space Administration,
Langley Field, Va., June 24, 1959.

APPENDIX

DETAILS OF CALCULATION

Equations of Motion

The equations of motion of the reentry vehicle under the action of gravity, lift, and drag may be written as

$$C_L \frac{\rho}{2} SV^2 - \frac{mg}{\left(1 + \frac{H}{R}\right)^2} \cos \theta = V\left(\dot{\theta} - \frac{V \cos \theta}{R + H}\right) \tag{A1a}$$

$$-C_D \frac{\rho}{2} SV^2 - \frac{mg}{\left(1 + \frac{H}{R}\right)^2} \sin \theta = m\dot{V} \tag{A1b}$$

for motion perpendicular to and along the flight path. In terms of altitude H and position angle ψ the motion is

$$V \sin \theta = \dot{H} \tag{A1c}$$

$$\frac{V \cos \theta}{R + H} = \dot{\psi} \tag{A1d}$$

In equations (A1), R is the radius of the earth and g the acceleration of gravity at the earth's surface. The earth and the atmosphere are considered to be radially symmetric and at rest. The assumed lack of rotation of the atmosphere is most nearly justified during a reentry in the polar regions. The coordinates are shown in figure 11. It was found convenient to nondimensionalize equations (A1) as follows:

The lift coefficient and wing loading are contained in the parameter λ which is defined as

$$\lambda = \frac{Sh_o}{2m} \rho C_L \tag{A2a}$$

The drag coefficient and wing loading are combined in the parameter δ where

$$\delta = \frac{Sh_o}{2m} \rho C_D \tag{A2b}$$

The dimensionless velocity is

$$\nu = \frac{V}{V_s} \tag{A2c}$$

where

$$V_s^2 = \frac{gR}{1 + D} \qquad \left(D = \frac{h_o}{R}\right) \tag{A2d}$$

is the square of the gravitational $(C_L = C_D = 0)$ satellite speed at the arbitrary reference altitude h_o.

The dimensionless acceleration of gravity is

$$\chi = \frac{D(1 + D)}{(1 + D\eta)^2} \tag{A2e}$$

The dimensionless distance from the center of the earth is

$$\frac{l}{\omega} = \frac{1 + D\eta}{D} \tag{A2f}$$

The dimensionless altitude is

$$\eta = \frac{H}{h_o} \tag{A2g}$$

The nondimensional equations of motion may now be written as

$$\lambda\nu^2 - (\chi - \omega\nu^2)\cos\theta = \nu\theta' \tag{A3a}$$

$$\delta\nu^2 - \chi \sin\theta = \nu' \tag{A3b}$$

$$\nu \sin\theta = \eta' \tag{A3c}$$

$$\omega\nu \cos\theta = \psi' \tag{A3d}$$

Primes denote differentiation with respect to a timelike variable τ

$$\tau = \frac{V_s t}{h_o}$$

Orbital Altitude

Setting $\delta = 0$ in equations (A3) yields the equations of the phugoid motion with zero drag and finite lift coefficient. The circular motion at the orbital altitude $\bar{\eta}$ is defined by also setting $\theta = \theta' = 0$ in equation (A3). This relationship gives the variation of orbital speed with altitude as

$$\bar{\nu}^2 = \frac{\bar{X}}{\bar{\omega} + \bar{\lambda}} \tag{A4}$$

In order to relate orbital altitude to the energy constant, a dimensionless energy constant Γ is defined as

$$\Gamma = \frac{T + W}{\frac{1}{2} m V_s^2} = \nu^2 - 2\frac{X}{\omega} \tag{A5}$$

Substituting equation (A4) into equation (A5) gives

$$\Gamma + 2\frac{\bar{X}}{\bar{\omega}} = \frac{\bar{X}}{\bar{\omega} + \bar{\lambda}} \tag{A6}$$

Equation (A6) implicitly defines $\bar{\eta}$ as a function of Γ. It was solved by iteration.

Machine Computation

The equations of motion (A1) were integrated by an IBM 704 electronic data processing machine. Gill's modification of Kutta's method (ref. 7) was used. This method is a fourth-order approximation in the integration interval $\Delta\tau$. The arbitrary reference height h_o was chosen as 2×10^5 feet which made $\Delta\tau$, chosen as 0.05, equal to about 0.39 second.

After the vehicle passed minimum altitude, the machine received special instructions involving Kepler's law of areas. A nondimensional form of Kepler's law may be written as

$$(1 + D\eta)\nu \cos\theta = K \tag{A7a}$$

The instantaneous values of Γ and K fix the gravitational orbit for a coast which starts at any instant. The angle $\bar{\theta}$ at which the vehicle crosses $\bar{\eta}$ in the coast is found with the rewritten law of Kepler from

$$\sin \bar{\theta} = -\sqrt{1 - \frac{K^2}{(1 + D\bar{\eta})^2 \bar{\nu}^2}} \tag{A7b}$$

The negative sign of the root indicates that the vehicle is descending past $\bar{\eta}$. The altitude $\bar{\eta}$ is found by iteration of equation (A6) in the form

$$\bar{\lambda} = \bar{\omega}\left(\frac{\bar{\chi}/\bar{\omega}}{\Gamma + 2\frac{\chi}{\omega}} - 1\right) \tag{A8}$$

When equation (A7b) begins to produce real values of $\bar{\theta}$, the machine evaluated the function F which may be written

$$F = -\bar{\nu} \sin \bar{\theta} + \bar{\eta}' \tag{A9a}$$

The value of $\bar{\nu}$ was determined from equation (A6) by using Γ and $\bar{\eta}$. The value of $\bar{\eta}'$ is given by

$$\bar{\eta}' = \frac{-\Gamma'}{\bar{\omega}\left\{\Gamma + \frac{\left(\Gamma + 2\frac{\bar{\chi}}{\bar{\omega}}\right)^2}{\bar{\chi}}\left[\bar{\lambda} + \frac{1}{\bar{\omega}}\left(\frac{d\lambda}{d\eta}\right)_{\eta=\bar{\eta}}\right]\right\}} \tag{A9b}$$

with

$$\Gamma' = -2\delta\bar{\nu}^3 \tag{A9c}$$

When F changed sign, the lift and drag were suppressed and the coast maneuver was underway. Initially, the machine restored the lift at $\eta = \bar{\eta}$. Since the cutoff and restoration are both always late by $\Delta\tau/2$ on the average, the descents were too steep and the altitude too low at restoration. Slightly better results were obtained by restoring the lift slightly sooner on the condition $\eta' = \bar{\eta}'$ which was at too high an altitude. With infinite precision, of course, the distinction between the conditions $\eta = \bar{\eta}$ and $\eta' = \bar{\eta}'$ must disappear.

The density altitude relation used was that of the ARDC atmosphere. (See ref. 6.) For convenience in evaluating $\bar{\eta}'$, the tables were faired by polynomial segments of the following form

$$\log_e \rho = A_i + B_i(\eta - \eta_i) + C_i(\eta - \eta_i)^2 + D_i(\eta - \eta_i)^3 \tag{A10}$$

The coefficients A_i, B_i, C_i, and D_i used are shown in table II.

REFERENCES

1. Eggers, Alfred J., Jr., Allen, H. Julian, and Neice, Stanford E.: A Comparative Analysis of the Performance of Long-Range Hypervelocity Vehicles. NACA TN 4046, 1957. (Supersedes NACA RM A54L10.)

2. Allen, H. Julian, and Eggers, A. J., Jr.: A Study of the Motion and Aerodynamic Heating of Ballistic Missiles Entering the Earth's Atmosphere at High Supersonic Speeds. NACA Rep. 1381, 1958. (Supersedes NACA TN 4047.)

3. Chapman, Dean R.: An Approximate Analytical Method for Studying Entry Into Planetary Atmospheres. NACA TN 4276, 1958.

4. Ferri, Antonio, Feldman, Lewis, and Daskin, Walter: The Use of Lift for Re-entry From Satellite Trajectories. Jet Propulsion, vol. 27, no. 11, Nov. 1957, pp. 1184-1191.

5. Lees, Lester, Hartwig, Frederick W., and Cohen, Clarence B.: The Use of Aerodynamic Lift During Entry into the Earth's Atmosphere GM-TR-0165-00519, Space Tech. Labs., Inc., Nov. 20, 1958.

6. Minzner, R. A., and Ripley, W. S.: The ARDC Model Atmosphere, 1956. Air Force Surveys in Geophysics No. 86 (AFCRC TN-56-204), Geophysics Res. Dir., AF Cambridge Res. Center (Bedford, Mass.), Dec. 1956. (Available as ASTIA Doc. 110233.)

7. Gill, S.: A Process for the Step-by-Step Integration of Differential Equations in an Automatic Digital Computing Machine. Proc. Cambridge Phil. Soc., vol. 47, pt. 1, Jan. 1951, pp. 96-108.

TABLE I

AERODYNAMIC CHARACTERISTICS OF ASSUMED VEHICLES

$\left[C_D = 0.004 + 2.5C_L^2\right]$

$\frac{L}{D}$	C_L	C_D	W/C_DS for -	
			W/S = 100	W/S = 20
5	0.040	0.008	12,500	2,500
4	.080	.020	5,000	1,000
3	.120	.040	2,500	500
2	.192	.096	1,044	209
1	.396	.396	253	50.5
$\frac{1}{2}$	.798	1.596	62.7	12.5

TABLE II

COEFFICIENTS OF POLYNOMIAL

$$\log_e \rho = A_i + B_i(\eta - \eta_i) + C_i(\eta - \eta_i)^2 + D_i(\eta - \eta_i)^3$$

$$\left[\eta_i \leq \eta \leq \eta_{i+1}\right]$$

i	η_i	A_i	B_i	C_i	D_i
1	0	-6.0419581	-6.059732	-3.333864	-9.814176
2	.25	-7.9186041	-7.566822	-1.4024112	3.3035072
3	.50	-10.346343	-9.6486200	3.829456	-1.626816
4	.75	-12.544576	-8.0389200	7.790864	-15.933504
5	1.00	-14.316338	-7.131020	-.907168	-11.900672
6	1.25	-16.341739	-9.815980	-2.177088	.700608
7	1.50	-18.920855	-10.773160	1.642864	5.514816
8	1.75	-21.425297	-8.917700	3.731328	-1.618688
9	2.00	-23.446806	-7.355540	-.991136	7.926336
10	2.25	-25.223788	-6.364920	4.484928	-2.865088
11	2.50	-26.579477	-4.659660	2.451312	-1.267072
12	2.75	-27.610983	-3.671580	1.171888	1.645312
13	3.00	-28.429927	-2.777140	.583872	-.141632
14	3.25	-29.089933	-2.511760	.480336	-.107456
15	3.50	-29.689531	-2.291740	.407552	-.106112
16	3.75	-30.238652	-2.107860	.411648	-.324608
17	4.00	-30.744961	-1.962900	0	0

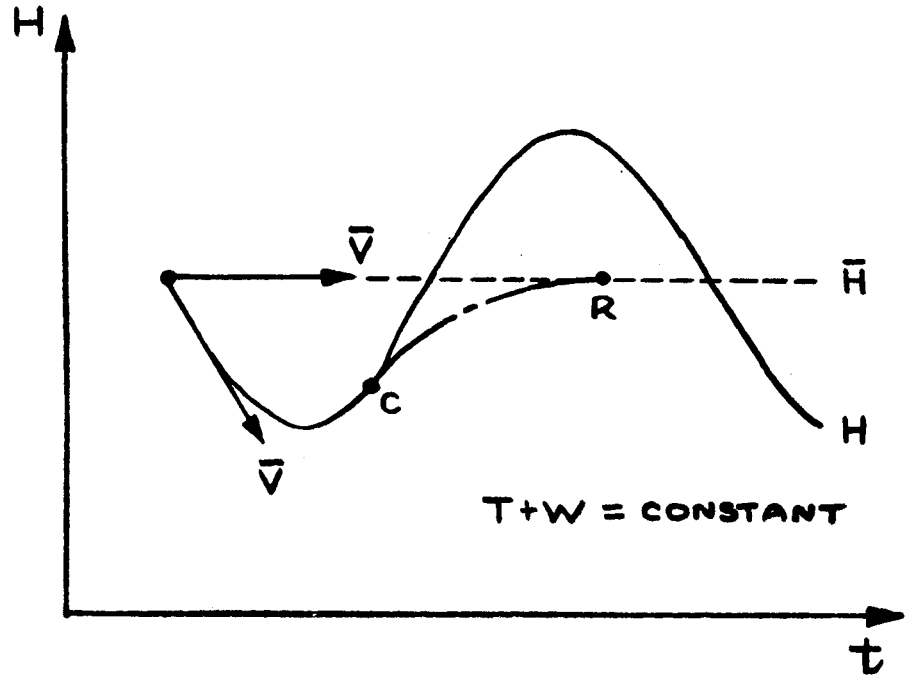

Figure 1.- Skipping motion for zero drag. The symbol C denotes lift cutoff and R, the lift restoration.

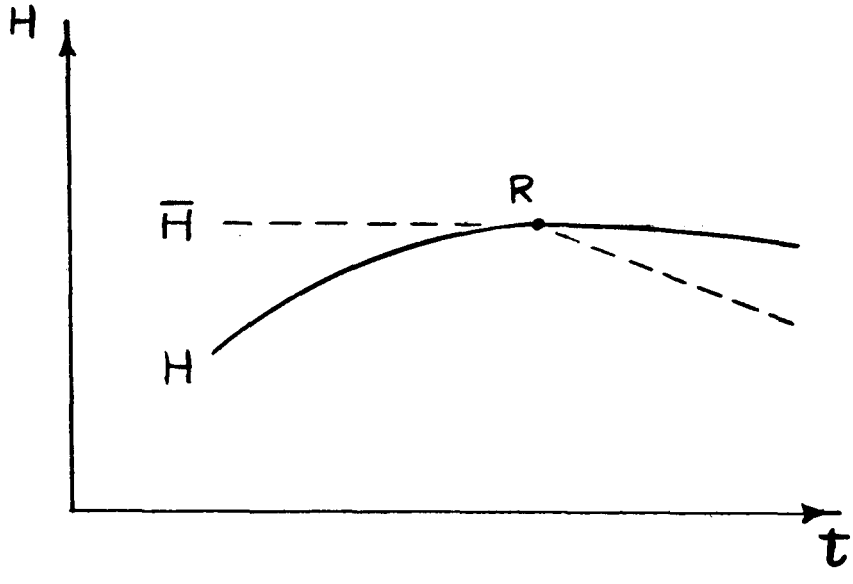

Figure 2.- Effect of finite drag at lift restoration.

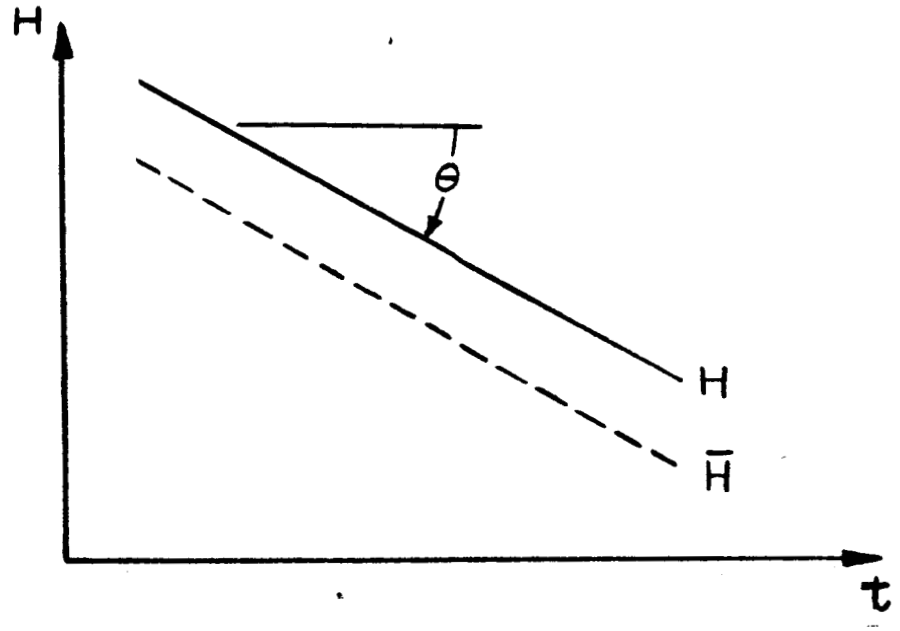

Figure 3.- Boundary conditions for the glide. $\dot{H} = \dot{\bar{H}}$; $\dot{\theta} = 0$.

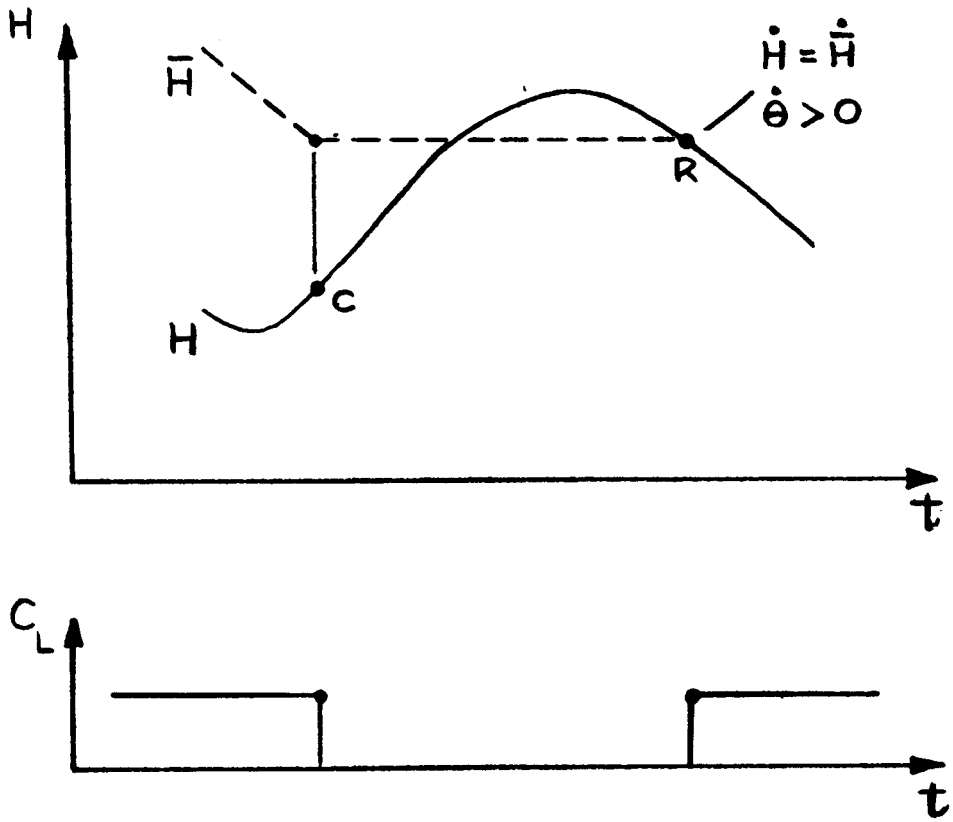

Figure 4.- Transfer maneuver with zero coast drag.

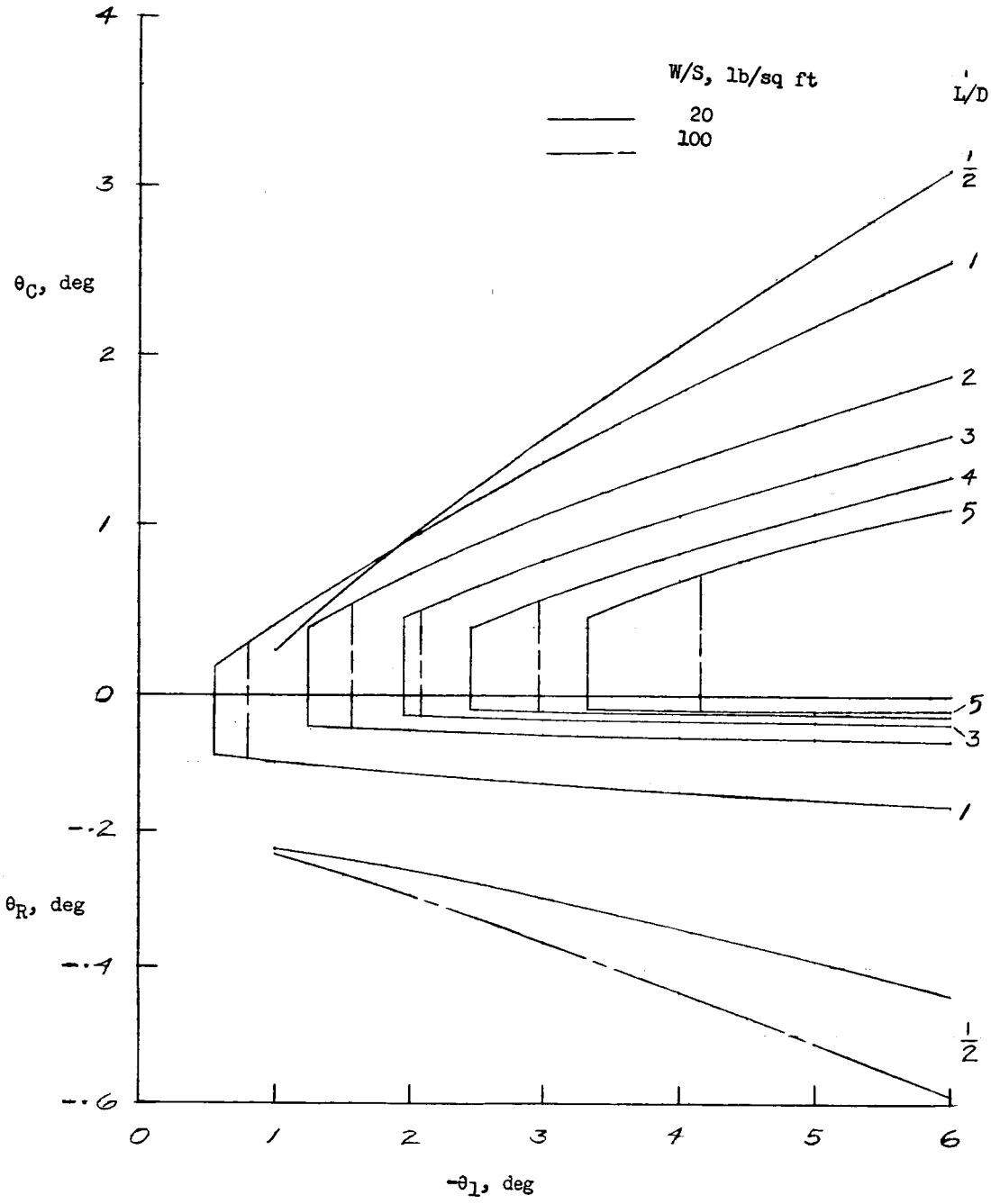

(a) V_1 = 25,900 ft/sec.

Figure 5.- Variations of angles of cutoff and restoration of lift with reentry angle. H_1 = 350,000 ft.

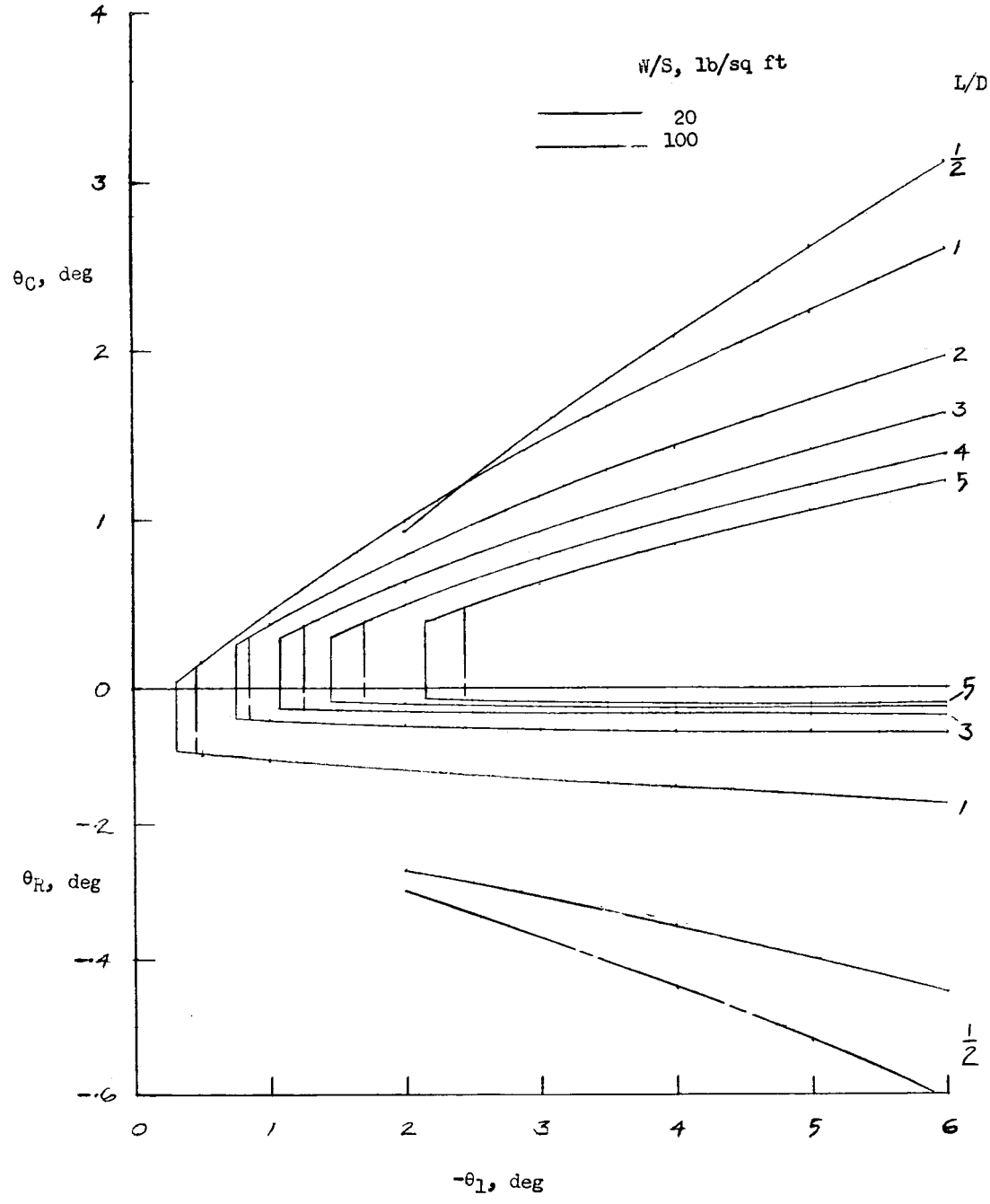

(b) V_1 = 25,800 ft/sec.

Figure 5.- Concluded.

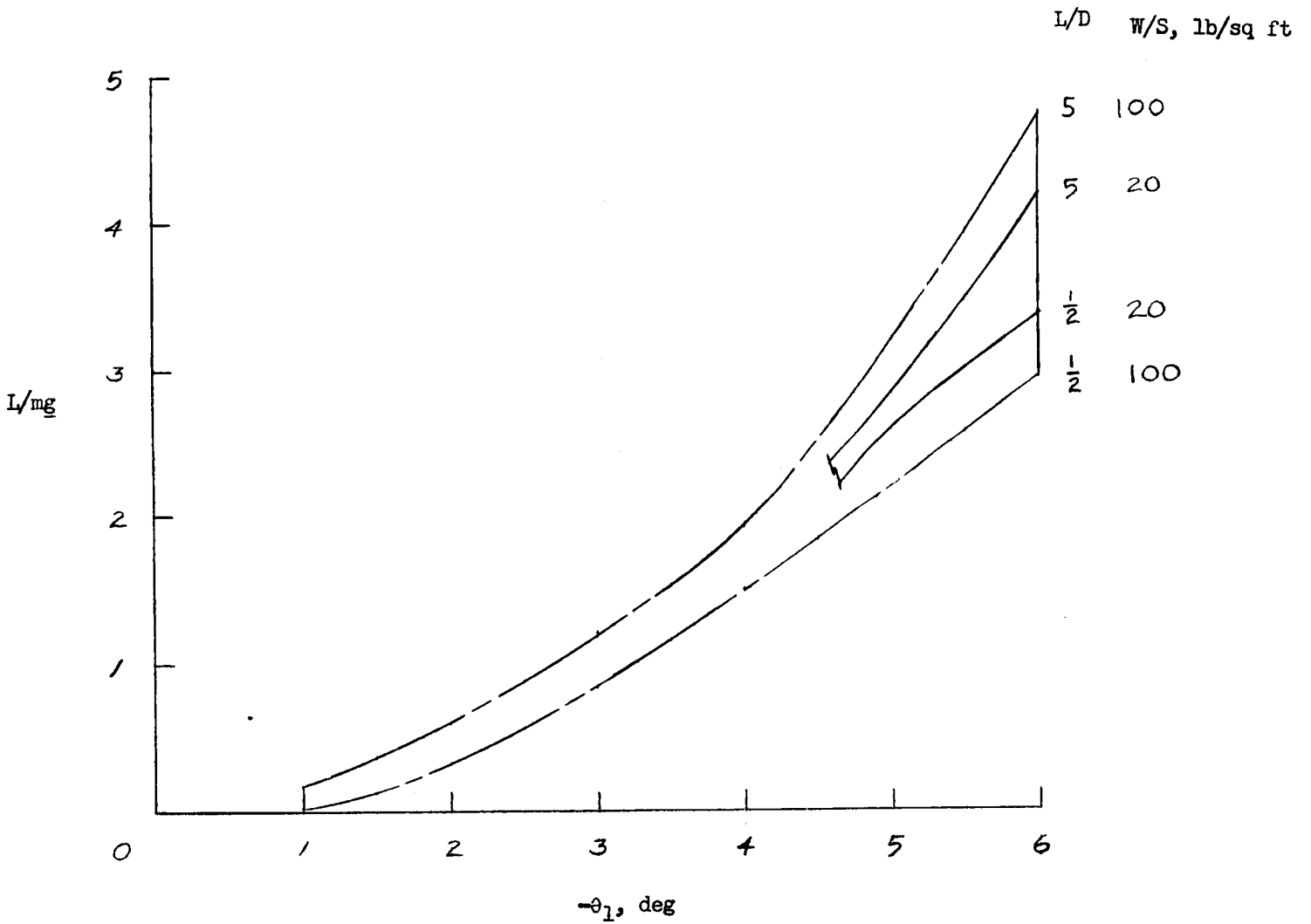

Figure 6.- Variation with reentry angle of maximum normal acceleration due to air loads V_1 = 25,900 and 25,800 ft/sec; H_1 = 350,000 ft.

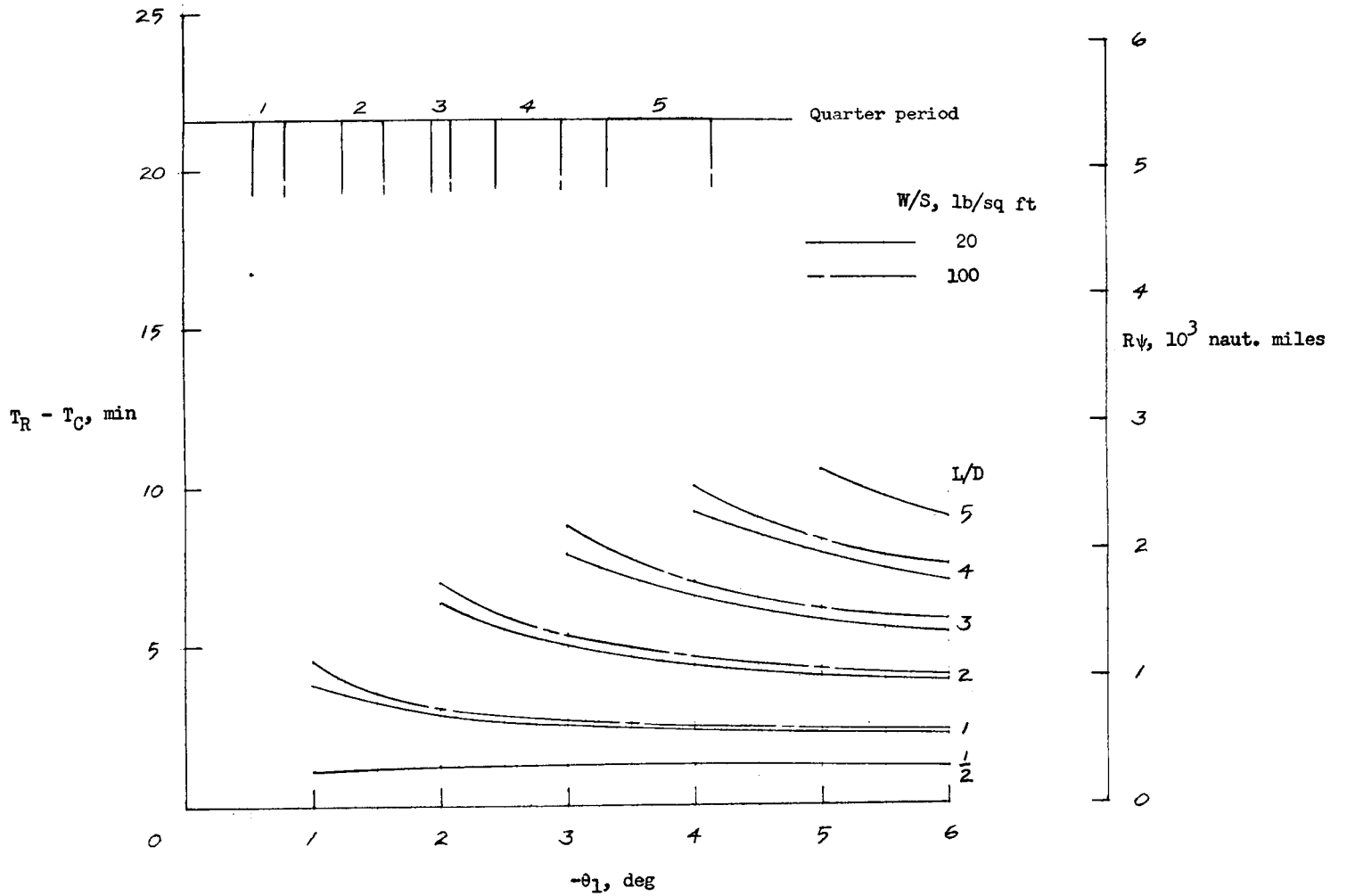

(a) V_1 = 25,900 ft/sec.

Figure 7.- Variation of coasting time and distance with reentry angle. H_1 = 350,000 ft.

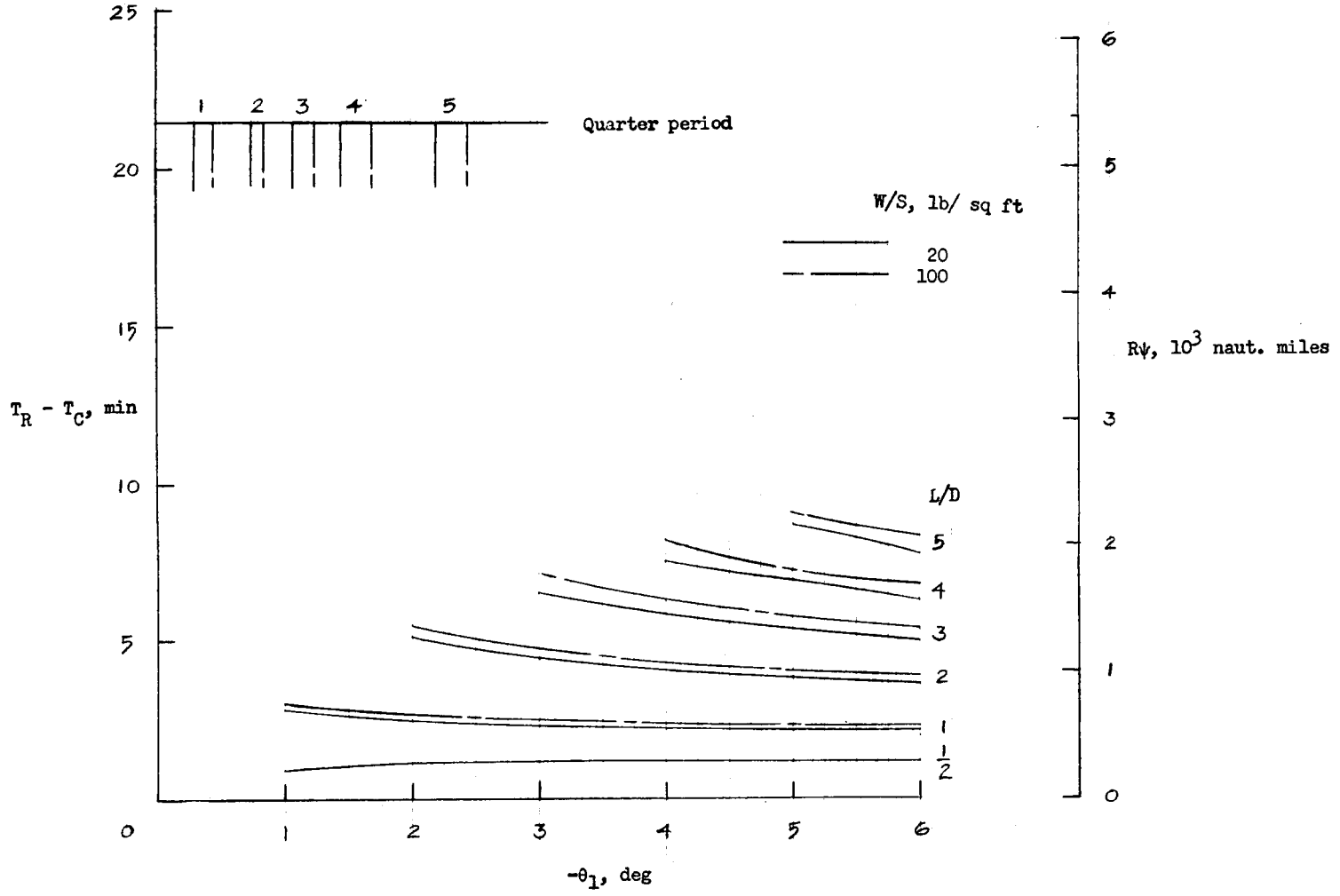

(b) V_1 = 25,800 ft/sec.

Figure 7.- Concluded.

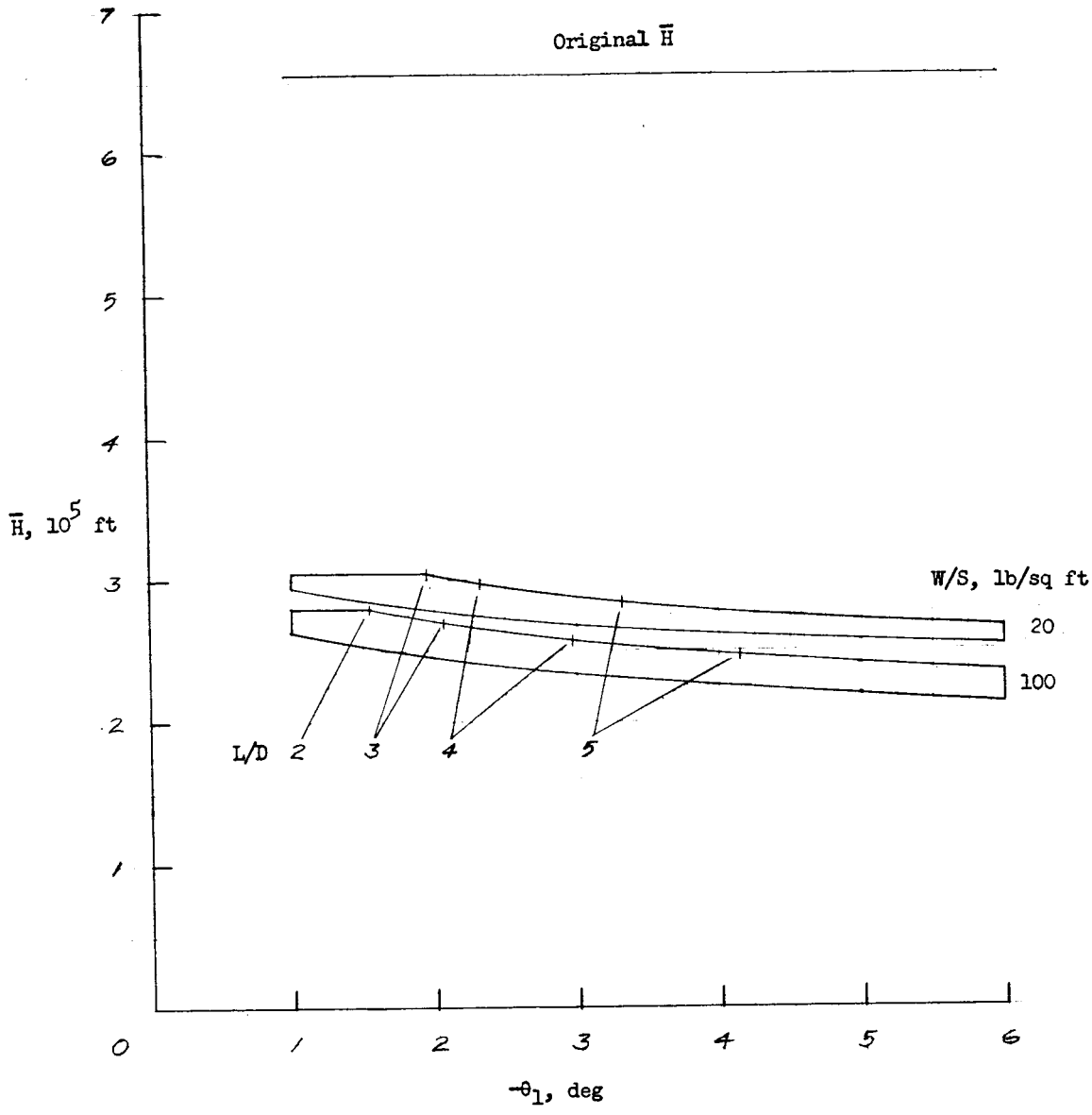

(a) V_1 = 25,900 ft/sec.

Figure 8.- Variation with reentry angle with orbital height at lift cut-off. H_1 = 350,000 ft.

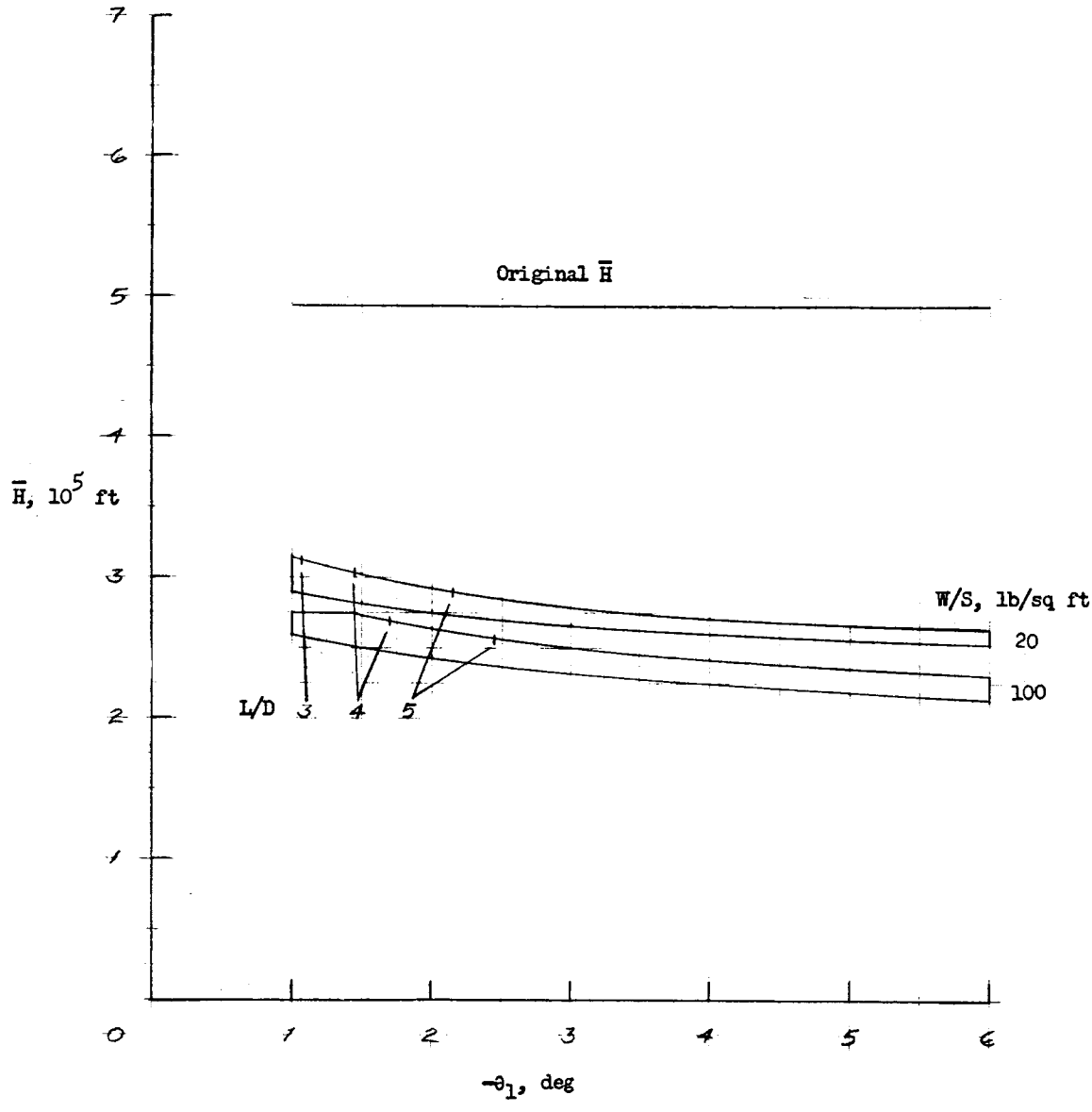

(b) V_1 = 25,800 ft/sec.

Figure 8.- Concluded.

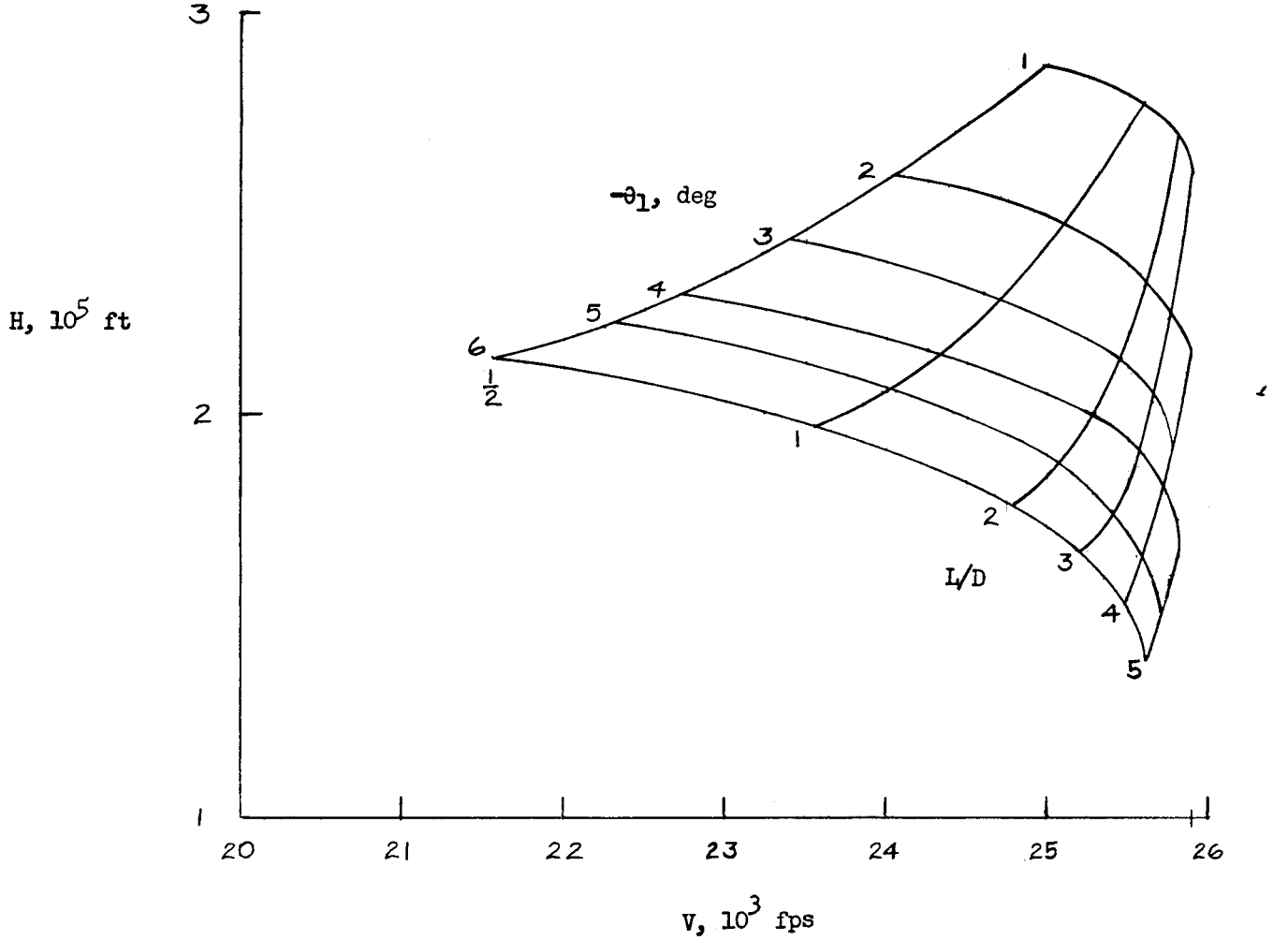

(a) W/S = 20 lb/sq ft; V_1 = 25,900 fps.

Figure 9.- Velocity and altitude at bottom of pullups.

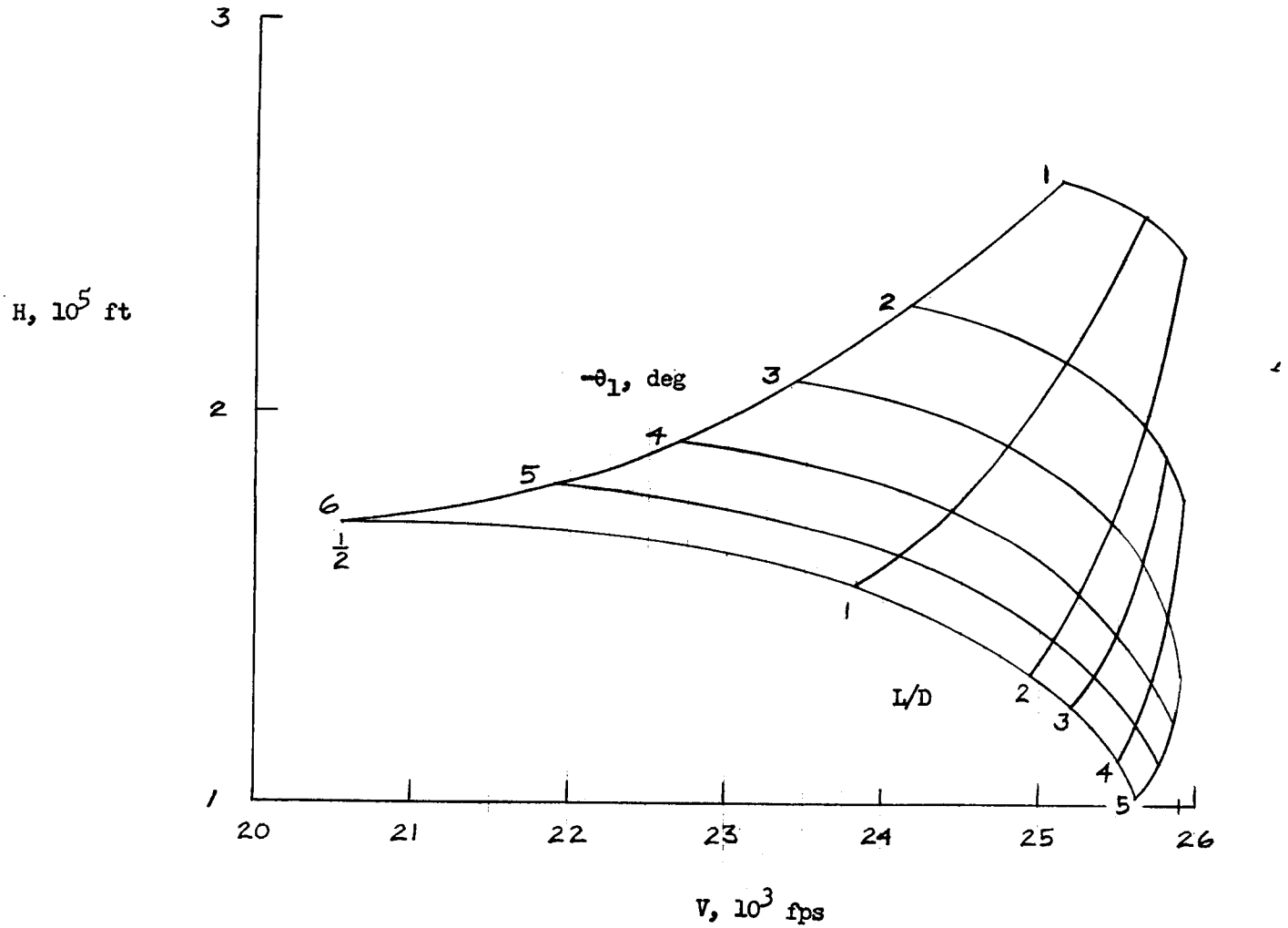

(b) W/S = 100 lb/sq ft; V_1 = 25,900 fps.

Figure 9.- Continued.

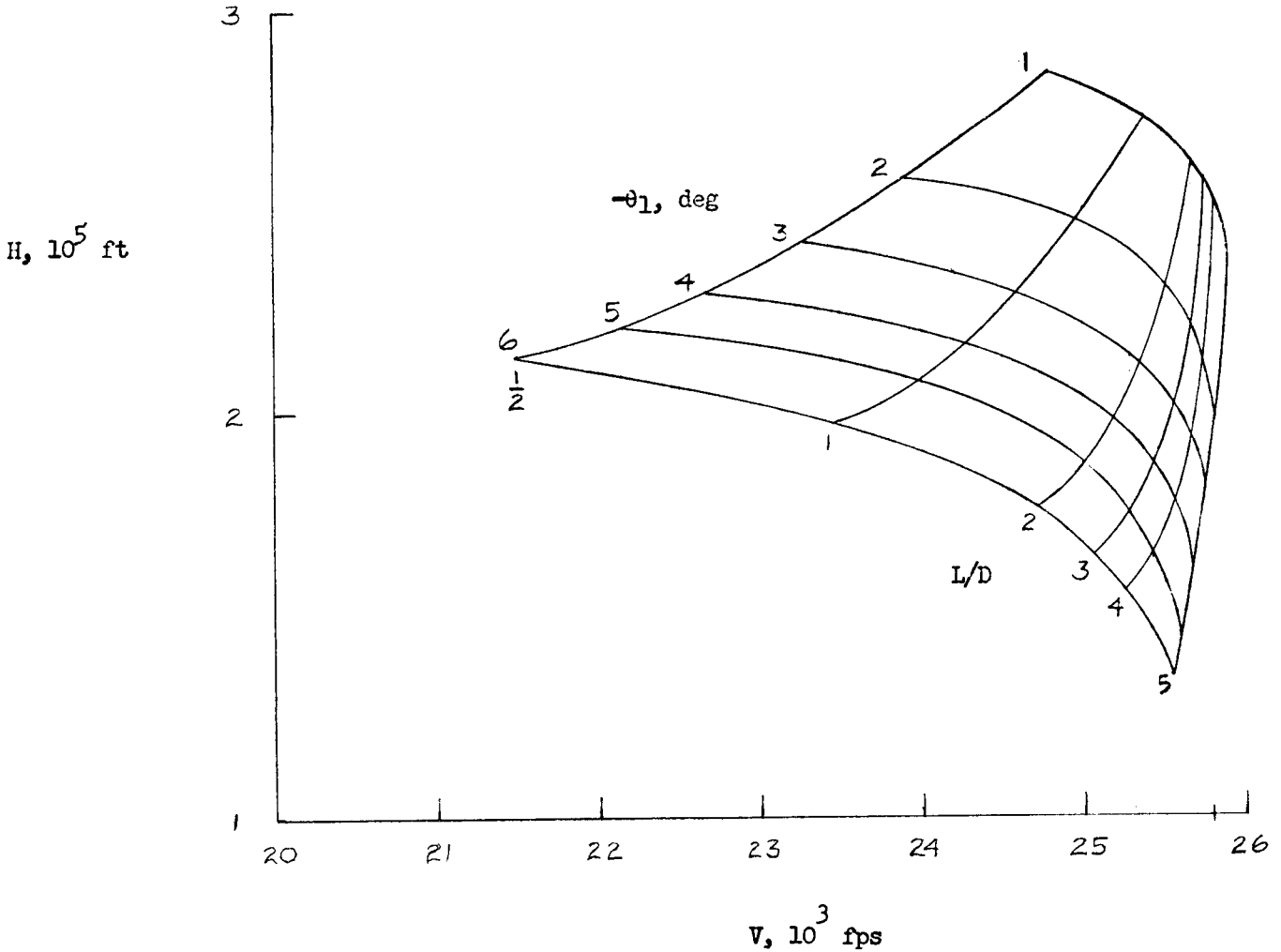

(c) W/S = 20 lb/sq ft; V_1 = 25,800 fps.

Figure 9.- Continued.

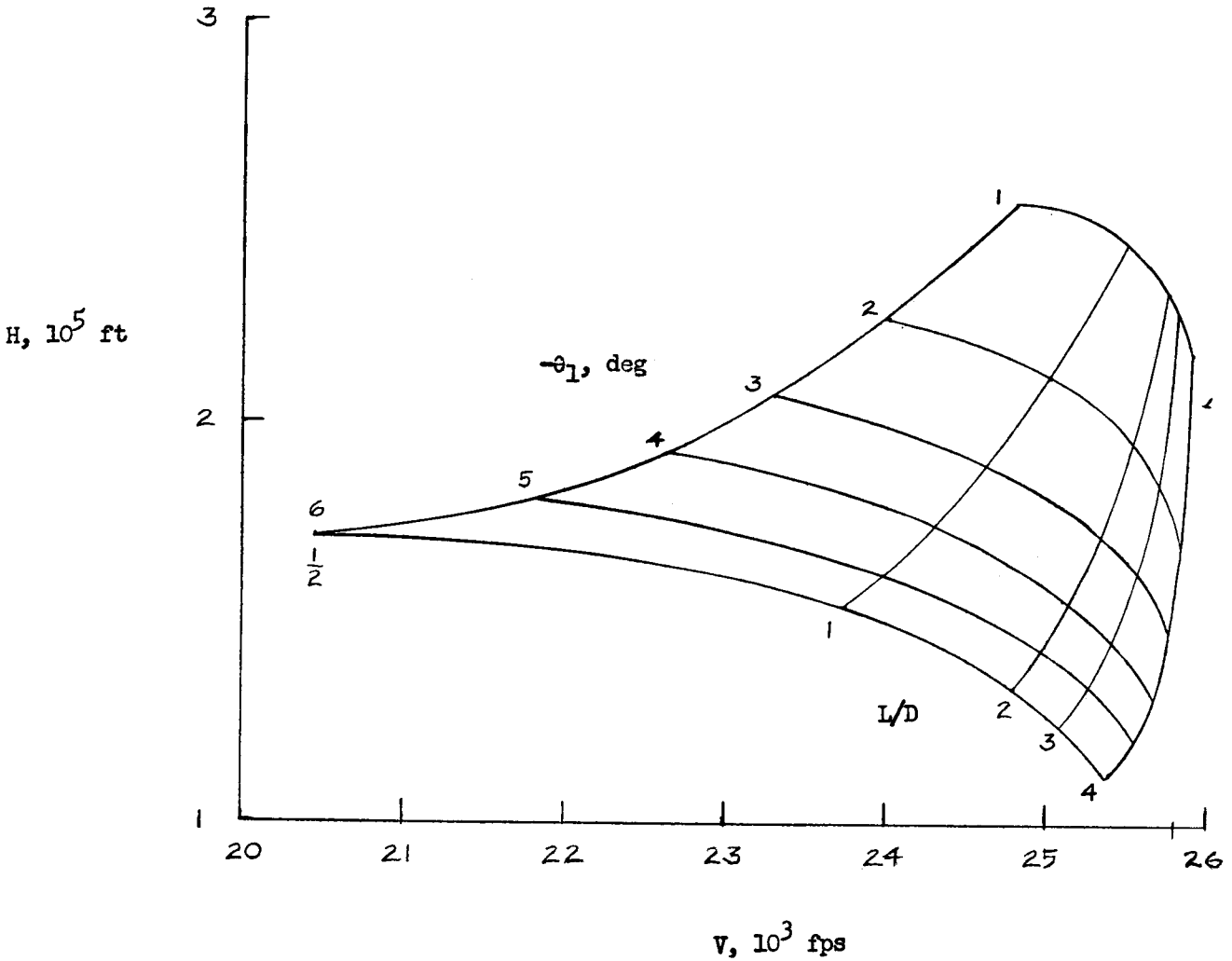

(d) W/S = 100 lb/sq ft; V_1 = 25,800 fps.

Figure 9.- Concluded.

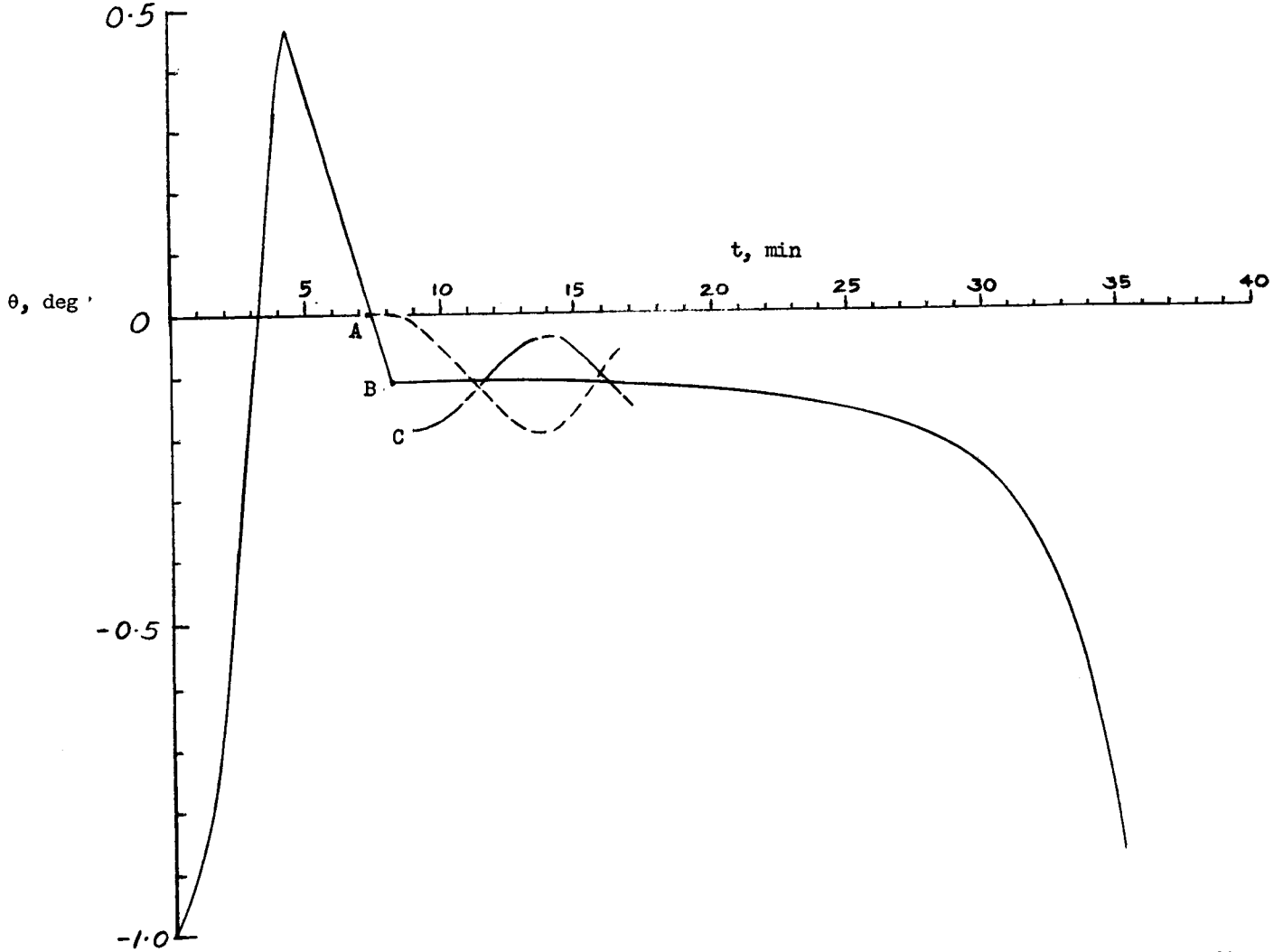

Figure 10.- Effect of improper lift cutoff. H_1 = 350,000 ft; V_1 = 25,900 ft/sec; W/S = 20 lb/sq ft; $C_L = C_D = 1$.

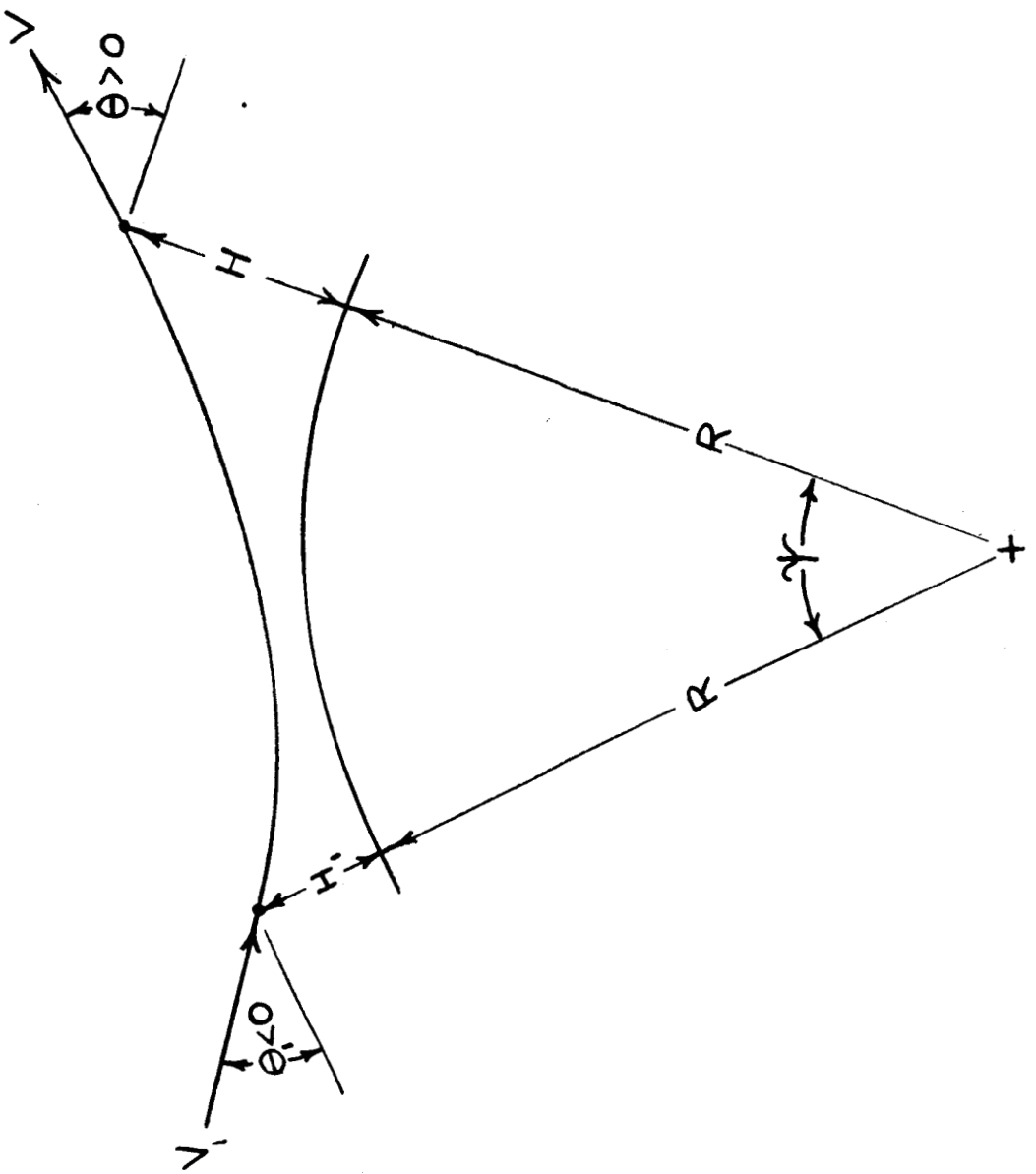

Figure 11.- Coordinate system.